JOURNAL OF SOLID STATE CHEMISTRY 67, 78–84 (1987)

Heat Capacity and Thermodynamic Functions of $Mn_xFe_{1-x}Cl_2 \cdot 4H_2O$, $x = 0.51$

D. L. SCHOCH, J. E. MOORE,* AND R. A. BUTERA†

Department of Chemistry, University of Pittsburgh, Pittsburgh, Pennsylvania 15260

Received March 12, 1986

The heat capacity of $Mn_xFe_{1-x}Cl_2 \cdot 4H_2O$ for $x = 0.51 \pm 0.005$ has been experimentally determined from 1.4 to 300°K. The smoothed heat capacity and thermodynamic functions $(H_T^0 - H_{10}^0)$ and $(S_T^0 - S_{10}^0)$ are reported over the temperature range 10 to 300 K. The value of S_{10}^0 is given based on theoretical fits to the experimental data below 10 K. The error in the tabulated values arising from the heat capacity data above 10 K is thought to be less than 1%. $Mn_xFe_{1-x}Cl_2 \cdot 4H_2O$, $x = 0.51$ is isostructural with $MnCl_2 \cdot 4H_2O$, but exhibits a Schottky anomaly similar to $FeCl_2 \cdot 4H_2O$. Separating the lattice and Schottky heat capacities yields a T^3 lattice constant of $1.413 \pm 0.028 \times 10^{-3}$ J/mole-K^4 and a Schottky doublet–triplet mean separation of 18.0 ± 0.5 K. The lattice constant is, within the quoted uncertainty, identical to the T^3 lattice constant of $MnCl_2 \cdot 4H_2O$. The Schottky level separation, however, is significantly greater than the 7.6 K separation found in $FeCl_2 \cdot 4H_2O$. This is presumably due to the change in chloride coordination from *trans* to *cis* in the present case. A cooperative transition just below the extent of the present data is thought to involve both the $\frac{5}{2}$ spin Mn^{2+} and the quasi-$\frac{1}{2}$ spin Fe^{2+} ions.

Introduction

Both $MnCl_2 \cdot 4H_2O$ and $FeCl_2 \cdot 4H_2O$ are well characterized compounds; structurally (*1–3*), thermodynamically (*4–6*), and magnetically (*6–10*). Recently, a system consisting of a co-precipitated mixture of equal proportions of $MnCl_2 \cdot 4H_2O$ and $FeCl_2 \cdot 4H_2O$ was studied, yielding Mössbauer and X-ray powder diffraction data (*11, 12*). Such a mixed crystal system is of interest in several regards.

Magnetically, both $MnCl_2 \cdot 4H_2O$ and $FeCl_2 \cdot 4H_2O$ order antiferromagnetically at temperatures of 1.62 and 1.10 K, respectively. However, the compounds represent quite different situations in the interplay between exchange and crystal field interactions. $MnCl_2 \cdot 4H_2O$ possesses an exchange and single ion anisotropy of comparable magnitude (*10*), while the zero-field splitting of Fe^{2+} in $FeCl_2 \cdot 4H_2O$ is approximately an order of magnitude greater than the exchange energy (*6*). To what extent these individual traits are preserved or modified in a mixed spin system is of general interest in the understanding of cooperative phenomena.

Structurally, $MnCl_2 \cdot 4H_2O$ belongs to the $P2_{1/n}$ space group with the chlorides occupying *cis* positions in the Mn^{2+} coordination shell, whereas $FeCl_2 \cdot 4H_2O$ belongs to the $P2_{1/c}$ space group with the chlorides occu-

* Present address: AT&T Bell Laboratories, Murray Hill, NJ 07974.

† To whom correspondence should be addressed.

0022-4596/87 $3.00

pying *trans* positions in the Fe^{2+} coordination shell. In a mixture, the chemically analogous but structurally different compounds provide an opportunity to study the effects of a structural variation in the metal coordination while maintaining the same chemical partners. In the present case, Fe^{2+} substitutes into the $MnCl_2 \cdot 4H_2O$ crystal structure to a level of nearly 50% without significant perturbation to the $MnCl_2 \cdot 4H_2O$ structure (*13*). Presumably in a sufficiently iron-rich mixture the Mn^{2+} would similarly adopt the $FeCl_2 \cdot 4H_2O$ structure. In support of this presumption is the occurrence of the unstable β-phase $MnCl_2 \cdot 4H_2O$. Obtained from supersaturated manganese chloride solutions, the β phase occurs frequently as large well formed crystals morphologically similar to $FeCl_2 \cdot 4H_2O$. Although these crystals rapidly decompose when disturbed (turn opaque and powder when removed from solution) and no structural determination has been reported to date, the β phase has been assumed isostructural with $FeCl_2 \cdot 4H_2O$ (*3, 14*).

The present work focuses on the low temperature magnetic and calorimetric effects of the $MnCl_2 \cdot 4H_2O$ structure on Fe^{2+}; however, it is apparent that the electronic states of the Fe^{2+} ion have changed as well. $FeCl_2 \cdot 4H_2O$ is a blue-green material while $MnCl_2 \cdot 4H_2O$ is a light pink. The $Mn_xFe_{1-x}Cl_2 \cdot 4H_2O$, $x = 0.51$, used in this study is nearly colorless showing only a faint pink hue for relatively thick sections of material. Specifically where the Fe^{2+} absorption bands have shifted has yet to be determined, but preliminary UV-visible spectra (300–800 nm) suggest that the predominant near infrared absorption peak of Fe^{2+} in $FeCl_2 \cdot 4H_2O$ has moved deeper into the infrared giving rise to the colorless appearance.

Presently, we report the smooth heat capacity and thermodynamic functions $(H_T^0 - H_{10}^0)$ and $(S_T^0 - S_{10}^0)$ over the 10 to 300 K temperature range for $Mn_xFe_{1-x}Cl_2 \cdot 4H_2O$, $x = 0.51$. Based on theoretical fits to the heat capacity data below 10 K and reasonable assumptions concerning an apparent cooperative transition below the extent of our data, a value for S_{10}^0 is obtained. Further investigation is required to firmly establish the existence and to characterize the behavior of the cooperative transition involving the $\frac{5}{2}$ spin Mn^{2+} and quasi-$\frac{1}{2}$ spin Fe^{2+} ions.

Sample Preparation and Assay

The $Mn_xFe_{1-x}Cl_2 \cdot 4H_2O$ used in this study was crystallized from a 50/50 mol% Mn^{2+}/Fe^{2+} chloride aqueous solution. The solution was prepared with distilled water purged with N_2(g) and well formed crystals of $MnCl_2 \cdot 4H_2O$ and $FeCl_2 \cdot 4H_2O$ obtained by recrystallization of reagent grade $MnCl_2 \cdot 4H_2O$ and $FeCl_2 \cdot 4H_2O$ (*15*). The use of well-formed crystals minimizes the uncertainty in the water stoichiometry of the starting materials. All manipulations involving the iron chloride or manganese/iron chloride solutions were performed under an inert atmosphere to avoid oxidation of the Fe^{2+}. Exposure to strong light sources was also avoided.

The actual crystallization of the $FeCl_2 \cdot 4H_2O$ starting material and the $Mn_xFe_{1-x}Cl_2 \cdot 4H_2O$ occurred at room temperature inside a dessicator with freshly baked molecular sieves serving as the dessicant. In the case of the $Mn_xFe_{1-x}Cl_2 \cdot 4H_2O$, initial crystallization yielded green diamond-shaped platelets morpholically similar to $FeCl_2 \cdot 4H_2O$. These crystals proved to be unstable when removed from solution and decomposed with characteristics similar to the β-phase $MnCl_2 \cdot 4H_2O$. Assay indicated these first crystals to be approximately 65% Fe^{2+}.

After the removal of the green crystals, clear hexagonal platelets began to crystallize. This second phase proved to be stable and morphologically similar to the stable α-phase $MnCl_2 \cdot 4H_2O$. Assay of the crystals

used in the present study indicated these clear platelets to be $Mn_xFe_{1-x}Cl_2 \cdot 4H_2O$, $x = 0.510 \pm 0.005$ (esd).

The forementioned analyses were performed using X-ray fluorescence measurements of the $K\alpha_1$ manganese and $K\beta_1$ iron peaks to yield relative Mn/Fe concentration ratios. A calibration was performed using known mixtures of $MnCl_2 \cdot 4H_2O$ and $FeCl_2 \cdot 4H_2O$. These known mixtures were completely dissolved, forced to dryness, and crushed to fine powder. Unknown samples were similarly treated. The estimated standard deviation (esd) of the calibration was approximately 0.5 mol%.

As an accuracy check of the X-ray fluorescence measurements, visible absorbance measurements were performed on a few of the samples. Using 1,10-phenanthroline which complexes both Fe^{2+} and Fe^{3+}, visible absorbance measurements allowed the absolute Fe^{2+} concentration to be determined (*16, 17*). The presence of the Fe^{3+} complex (spectrally distinct from the Fe^{2+} complex) was not detected in any of the assays and the Fe^{2+} concentrations were found in acceptable agreement with the X-ray fluorescence measurements.

The crystal structure of the $Mn_xFe_{1-x}Cl_2 \cdot 4H_2O$ used in this study has been determined to be isostructural with $MnCl_2 \cdot 4H_2O$ (13). Table I compares the unit cell dimensions of the two systems. The slightly smaller unit cell dimensions of $Mn_xFe_{1-x}Cl_2 \cdot 4H_2O$ can be attributed primarily to the temperature difference at which the structures were determined. The randomly distributed Fe^{2+} ions have substituted directly for the displaced Mn^{2+} ions.

TABLE I

	$Mn_xFe_{1-x}Cl_2 \cdot 4H_2O$ $x = 0.51$, $T = 80$ K (Ref. (*13*))	$MnCl_2 \cdot 4H_2O$ $T = RT$ (Ref. (*1*))
a	11.112 Å	11.186(6) Å
b	9.446 Å	9.513(5) Å
c	6.092 Å	6.186(2) Å
β	99.45°	99.74(4)°

Although no structural determinations have been performed on the initial unstable green phase, it seems likely that these crystals were isostructural with $FeCl_2 \cdot 4H_2O$, as has been the assumption in regard to β-$MnCl_2 \cdot 4H_2O$.

Apparatus

Two calorimeters were used in this study. The adiabatic calorimeter used for temperatures above 10 K has been described elsewhere (*18*). The sample size for this calorimeter was 33.0734 g of well-formed crystals with an average dimension of approximately 5 mm. For temperatures below about 15 K a pulse calorimeter was used. This calorimeter has also been previously described (*19*), and the sample was a single 0.3370-g crystal.

Results

Figure 1 shows the heat capacity data[1] below 20 K. The data from the adiabatic calorimeter are shown as bars indicating the initial and final temperatures of the individual heat capacity measurements. The heat capacity data from the pulse calorimeter are shown as dots centered on the average temperature of the individual measurements. The nominal temperature step size for the pulse calorimeter data is $T/20$. In

[1] See NAPS document 04416 for 6 pages of supplementary material. Order from ASIS/NAPS, Microfiche Publications, P.O. Box 3513, Grand Central Station, New York, NY 10163. Remit in advance $4.00 for microfiche copy or for photocopy, $7.75 up to 20 pages plus $0.30 for each additional page. All orders must be prepaid. Institutions and organizations may order by purchase order. However, there is a billing and handling charge for this service of $15. Foreign orders add $4.50 for postage and handling, for the first 20 pages, and $1.00 for each additional 10 pages of material. There is a $1.50 charge for postage for any microfiche orders.

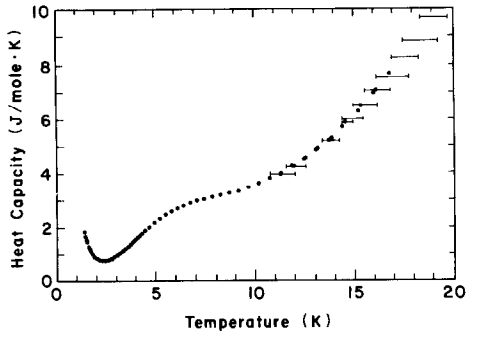

FIG. 1. Heat capacity for $Mn_xFe_{1-x}Cl_2 \cdot 4H_2O$, $x = 0.51$.

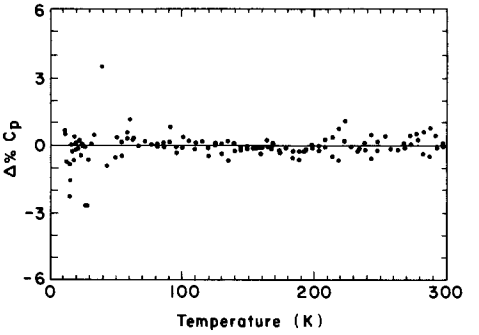

FIG. 3. Delta percent between smoothed heat capacity curve and experimental data for temperatures above 10 K.

Fig. 2 the heat capacity data from the adiabatic calorimeter are shown from 10 to 300 K. Due to the scale, the data are similarly shown as dots centered at the average temperature of the individual heat capacity measurements. The nominal temperature step size is $T/10$ for T less than 50 and 5 K for T at or above 50 K.

Our method of smoothing the experimental data involves the use of a draftman's spline, and has been detailed elsewhere (*4*). Figure 3 shows the percent deviation,

$$\Delta\%Cp = \frac{\text{Smooth Cp} - \text{Experimental Cp}}{\text{Smooth Cp}} \times 100\%, \quad (1)$$

for the data above 10 K. Table II gives the smooth heat capacity and thermodynamic functions $(H_T^0 - H_{10}^0)$ and $(S_T^0 - S_{10}^0)$ over the 10 to 300 K temperature range. The tabulated thermodynamic functions were obtained numerically from the smoothed heat capacity curve. The smoothed heat capacity data density used in these evaluations was sufficiently high so that insignificant error was introduced due to the numerical techniques.

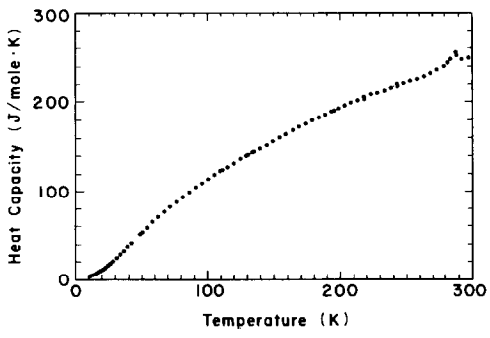

FIG. 2. Heat capacity for $Mn_xFe_{1-x}Cl_2 \cdot 4H_2O$, $x = 0.51$ for temperatures above 10 K.

Discussion

The low-temperature heat capacity shown in Fig. 1 is composed sequentially of the high-temperature tail of a cooperative transition apparently around 1 K, a Schottky anomaly peaking at 7 K, and finally domination by the lattice contribution about 10 K. $MnCl_2 \cdot 4H_2O$ has an antiferromagnetic transition at 1.62 K, but does not display a Schottky anomaly above this cooperative transition. $FeCl_2 \cdot 4H_2O$, however has a Schottky anomaly peaking at approximately 3 K in addition to a cooperative antiferromagnetic transition at 1.10 K. Friedberg *et al.* (*5*) modeled the $FeCl_2 \cdot 4H_2O$ Schottky as a doublet-triplet splitting of the Fe^{2+} spin levels, finding a mean separation of $\delta = 7.6$ K. In $Mn_xFe_{1-x}Cl_2 \cdot 4H_2O$ the Schottky anomaly is also attributed to the Fe^{2+}. Since the chloride coordination

TABLE II

SMOOTH THERMODYNAMIC FUNCTIONS FOR $Mn(0.51)Fe(0.49)Cl_2 \cdot 4H_2O$

T (K)	Cp (J/mole-K)	$H_T^0 - H_{10}^0$ (J/mole)	$S_T^0 - S_{10}^0$ (J/mole-K)
10.00	3.63	0.00	0.00
15.00	6.29	23.72	1.89
20.00	11.03	66.19	4.30
25.00	17.28	136.67	7.42
30.00	24.17	240.04	11.17
35.00	31.30	378.46	15.42
40.00	38.60	553.21	20.08
45.00	45.82	764.28	25.04
50.00	53.08	1,011.53	30.24
55.00	60.28	1,294.98	35.64
60.00	67.30	1,614.00	41.19
65.00	74.19	1,967.70	46.85
70.00	80.66	2,355.17	52.59
75.00	86.70	2,773.62	58.36
80.00	92.55	3,221.79	64.14
85.00	98.29	3,698.96	69.93
90.00	103.87	4,204.42	75.70
95.00	109.03	4,736.78	81.46
100.00	114.12	5,294.64	87.18
110.00	123.61	6,483.97	98.51
120.00	132.76	7,766.24	109.66
130.00	141.31	9,137.24	120.63
140.00	149.31	10,591.44	131.40
150.00	157.70	12,127.32	142.00
160.00	166.09	13,745.94	152.44
170.00	173.91	15,446.92	162.75
180.00	181.10	17,222.65	172.90
190.00	187.99	19,067.94	182.87
200.00	194.48	20,980.53	192.68
210.00	200.52	22,956.17	202.32
220.00	206.31	24,990.83	211.78
230.00	211.95	27,082.38	221.08
240.00	217.26	29,228.86	230.21
250.00	222.60	31,427.92	239.19
260.00	228.05	33,680.78	248.03
270.00	233.93	35,990.20	256.74
273.15	235.98	36,730.26	259.47
280.00	242.00	38,355.32	265.38
290.00	245.79	40,853.57	274.11
298.15	249.93	42,872.05	280.97
300.00	250.97	43,335.54	282.52

has changed, it is not surprising that the Schottky maximum has moved.

Following an analysis along the lines of Freidberg *et al.* (*5*), an approximate separation of the lattice and Schottky heat capacity contributions is carried out. Figure 4 is a plot of CpT^2 versus T^5 for the $Mn_xFe_{1-x}Cl_2 \cdot 4H_2O$ heat capacity data. Also shown in this figure for comparison are the corresponding curves for $MnCl_2 \cdot 4H_2O$ and $FeCl_2 \cdot 4H_2O$ (*4*, *5*). Although a linear region is seen to exist from approximately 12 to 16 K, the slope and intercept are only crude approximations to the T^3 lattice coefficient and the Schottky level separation, respectively. In the region from 12 to 16 K, the Schottky is not varying simply as T^{-2}, and the additional character modifies both the slope and intercept of the least-squares line. The slope does provide a starting point for a simple iterative separation of the lattice and Schottky contributions.

Using the value of the slope to remove an approximate T^3 lattice contribution, the remaining heat capacity is found to have a maximum at 7.05 K. Assuming a doublet–triplet splitting, $\delta = 2.538\ T_{max}$ giving a level separation of 17.9 K. With this value of δ, the aberrant T^{-2} behavior of the Schottky can be accounted for. Over the narrow temperature region of 12 to 16 K, this behavior can be approximated as a straight line on the CpT^2 versus T^5 plot with a slope of $0.103 \pm 0.013 \times 10^{-3}$ J/mole-K^4. This additional slope has been erroneously included in the T^3 lattice coefficient. Correcting the slope gives a lattice constant of $A = 1.413 \pm 0.028 \times 10^{-3}$ J/mole-K^4 for $Mn_xFe_{1-x}Cl_2 \cdot 4H_2O$, $x = 0.510 \pm 0.005$. At the present level of accuracy, this is the same as the $MnCl_2 \cdot 4H_2O$ T^3 lattice constant. Since the crystal structures are the same and the masses of Mn and Fe are nearly identical, this is an expected result. Figure 5 shows the final separation of the lattice and Schottky heat capacity contributions. The Schottky maximum is found at 7.10 ± 0.20 K corresponding to a doublet–triplet mean separation of 18.0 ± 0.5 K. The expression used to fit the Schottky shown in Fig. 5 is given in Eq. (2). The necessary scaling factor f to produce the fit is the mole fraction

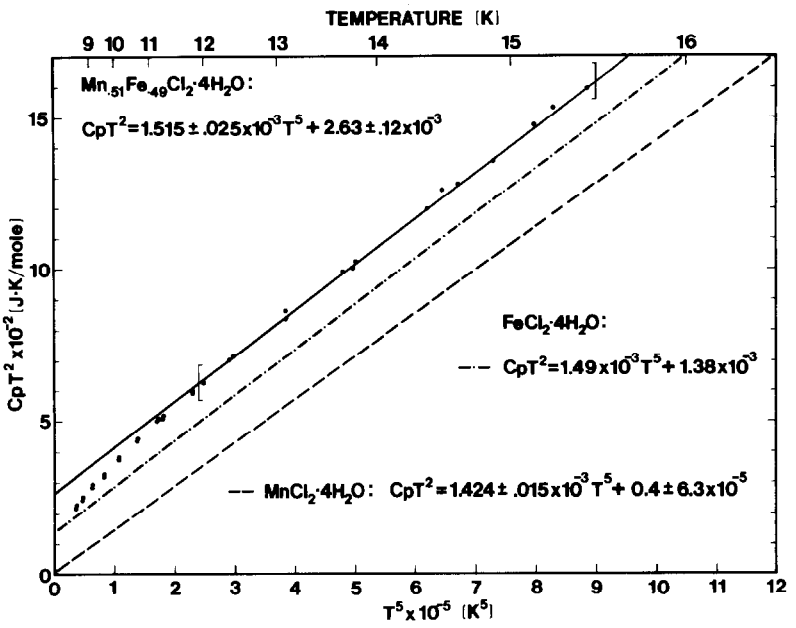

FIG. 4. CpT^2 versus T^5 plot for $Mn_xFe_{1-x}Cl_2 \cdot 4H_2O$, $x = 0.51$, yielding an approximate separation of the T^3 lattice and Schottky heat capacity contributions.

of iron found from the X-ray fluorescence assay.

$$Cp_{Schottky} = f \cdot 6R \frac{\delta^2}{T^2} \frac{\exp(\delta/T)}{(2\exp(\delta/T) + 3)^2} \qquad (2)$$

$$f = 0.49.$$

Throughout the analysis, the additional splitting of the doublet and triplet levels have been ignored. The local symmetry of the Fe^{2+} is sufficiently low that all degeneracies are expected to be removed. From the location of the apparent cooperative transition, the doublet splitting should be of the order 1 K, as in the case of $FeCl_2 \cdot 4H_2O$. This relatively small splitting should not significantly degrade the present approximation. The deviation of the data in the 10 to 15 K region, however, would suggest that the triplet splittings are not negligibly small. Above 15 K the T^3 lattice approximation begins to over estimate the true lattice contribution and thus it is difficult to draw further conclusions about the Schottky anomaly.

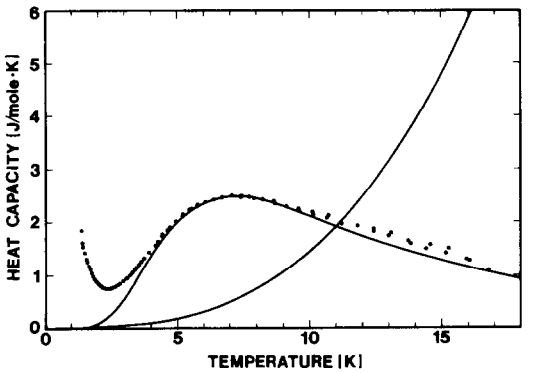

FIG. 5. Final separation of T^3 lattice and Schottky heat capacity contributions. The T^3 lattice curve shown has been removed from the data.

Based on the previous fits shown in Fig. 5 and reasonable assumptions regarding the cooperative transition below the extent of the present data, and approximate value of S_{10}^0 can be obtained. The cooperative transition is expected to involve both the $\frac{5}{2}$ spin Mn^{2+} and the Fe^{2+} doublet levels. At a temperature of 10 K these entropy contributions

should be nearly complete yielding 10.42 ± 0.04 J/mole-K. The quoted uncertainty is based on the 0.5 mol% esd assay of the individual metal ions, but assumes the combined metal stoichiometry is correct. Integrating the lattice and Schottky (numerically) contributions to 10 K yields 0.471 ± 0.009 J/mole-K and 2.36 ± 0.08 J/mole-K, respectively. Summing the individual contributions gives $S^0_{10} = 13.25 \pm 0.09$ J/mole-K.

If the preceding analyses are correct, general expectations for other Mn/Fe ratios can be stated. Mixtures with less Fe^{2+} should still possess a Schottky anomaly peaking around 7 K and the magnitude of this feature should scale with the iron content. The cooperative transition, however, should move to higher temperatures approaching 1.62 K in the limit of negligible Fe^{2+}. The presence of the Fe^{2+} appears to decrease the magnetic interaction strength leading to a lowering of the cooperative transition temperature. Whether this is simply due to the presence of the reduced spin moment of Fe^{2+} (quasi-$\frac{1}{2}$ spin) or a more complicated spin interaction scheme is not clear from the present work. For the complementary situation where Mn^{2+} enters the $FeCl_2 \cdot 4H_2O$ structure, the gross effects in regard to the heat capacity will be less noticeable. If the Mn^{2+} spin levels are less perturbed in the $FeCl_2 \cdot 4H_2O$ structure, as is the case for Fe^{2+}, the reduced spin splitting will have a minor impact on the already exchange-dominated magnetic interaction. Perhaps of greater interest would be the changes in magnetic interaction due to the new coordination of the chlorides and the effects on the exchange pathways.

References

1. Z. M. ELSAFFAR AND G. M. BROWN, *Acta Crystallogr. Sect. B* **27,** 66 (1971).
2. J. J. VERBIST, W. C. HAMILTON, T. F. KOETZEL, AND M. S. LEHMANN, *J. Chem. Phys.* **56,** 3257 (1972).
3. A. ZALKIN, J. D. FORRESTER, AND D. H. TEMPLETON, *Inorg. Chem.* **3,** 529 (1964).
4. J. E. MOORE AND R. A. BUTERA, *J. Solid State Chem.* **59,** 81 (1985).
5. S. A. FRIEDBERG, A. F. COHEN, AND J. H. SCHELLENG, *J. Phys. Soc. Jpn.* **17** (Suppl. B-1), 515 (1962).
6. C. A. RAQUET AND S. A. FRIEDBERG, *Phys. Rev. B* **6,** 4301 (1972).
7. W. F. GIAUQUE, E. W. HORNUNG, G. E. BRODALE, AND R. A. FISHER, *J. Chem. Phys.* **52,** 3936 (1970).
8. R. A. BUTERA AND D. R. RUTTER, *J. Appl. Phys.* **49,** 1344 (1978).
9. R. A. BUTERA, R. J. MOSKAITIS, D. R. RUTTER, AND R. T. OBERMYER, *J. Appl. Phys.* **50,** 1847 (1979).
10. J. E. RIVES AND V. BENEDICT, *Phys. Rev. B* **12,** 1908 (1975).
11. B. Y. ENWIYA, J. SILVER, AND I. E. G. MORRISON, *J. Chem. Soc. Dalton Trans.*, 2231 (1982).
12. B. Y. ENWIYA, J. SILVER, AND I. E. G. MORRISON, *J. Chem. Soc. Dalton Trans.*, 2581 (1983).
13. H. HOPE AND D. L. SCHOCH, *Acta Crystallogr.*, in press.
14. M. ABKOWITZ AND A. HONIG, *Phys. Rev.* **136,** A1003 (1964).
15. ACS Reagent Grade, Fisher Scientific Co., Fairlawn, NJ 07410.
16. A. E. HARVEY, J. A. SMART, AND E. S. AMIS, *Anal. Chem.* **27,** 26 (1955).
17. Z. MARCZENKO, "Spectrophotometric Determination of the Elements," Halsted, New York, 1976.
18. D. J. GERMANO, R. A. BUTERA, S. G. SANKAR, AND K. A. GSCHNEIDER, JR., *J. Appl. Phys.* **50,** 7495 (1979).
19. J. E. MOORE AND R. A. BUTERA, *J. Solid State Chem.* **60,** 188 (1985).